Eksakta : Berkala Ilmiah Bidang MIPA
VOLUME 27 NO 03 2026, pp 415-430
ISSN : Print 1411-3724 — Online 2549-7464
DOI : https://doi.org/10.24036/eksakta/vol27-iss03/703

Eksakta
Berkala Ilmiah Bidang MIPA
http://www.eksakta.ppj.unp.ac.id/index.php/eksakta

Article

Fluid Flow Analysis in Cisarua Hot Spring, South Lampung: A Study Using Geoelectric and Induced Polarization Methods

Article Info

Article history :
Received May 26, 2026
Revised June 18, 2026
Accepted June 22, 2026
Published June 30, 2026

Keywords :
Resistivity,
chargeability,
geothermal,
polarization methods

Fadhiah Nurul Aini[1*], Joan Margareth Sihol Marito S.[1], Selvi Misnia Irawati[1]

[1]Department of Geophysical Engineering, Faculty of Industrial Technology, Institut Teknologi Sumatera, Lampung, Indonesia

Abstract. Characterization of subsurface hydrothermal fluid flow pathways is essential for exploration and sustainable development of fault-controlled, non-volcanic geothermal systems. The Cisarua Hot Spring in Natar District, South Lampung, is a non-volcanic geothermal system controlled by the northwest-southeast trending Lampung–Panjang Fault; however, the hydraulic connectivity between the old well and new well manifestations has not been previously demonstrated geophysically. This study presents the first integrated Electrical Resistivity Tomography (ERT) and Induced Polarization (IP) investigation to map subsurface connectivity between both manifestation sources, aiming to identify hydrothermal fluid pathways and determine the hydraulic interconnection between the two wells. A Wenner–Schlumberger survey was conducted along four 235 m measurement lines with a maximum investigation depth of 44.65 m. Inversion results identify two principal lithologies: tuffaceous clay (resistivity <20 Ωm) and tuffaceous sand (20–33.6 Ωm). Zones of low resistivity coupled with elevated chargeability (>20 ms) on profiles 1 and 3 indicate active hydrothermal fluid pathways structurally controlled by the Lampung–Panjang Fault, with hydrothermally altered clay forming a confining layer above the reservoir. Results confirm that both wells constitute a single, internally connected hydrothermal system linked by a northwest-southeast trending fluid migration pathway along the fault zone.

Corresponding Author :
Fadhiah Nurul Aini
Department of Geophysical Engineering, Faculty of Industrial Technology,
Institut Teknologi Sumatera, South Lampung, Indonesia
Email : fadhiahnurulaini@gmail.com

1. Introduction

Indonesia possesses substantial geothermal energy potential owing to its location along the Ring of Fire, characterized by intense volcanic and tectonic activity [1-3]. These conditions facilitate the formation of geothermal systems, which are commonly indicated by various surface manifestations such as hot springs, fumaroles, and hydrothermal alteration zones [4-6]. The presence of such manifestations is frequently associated with local geological conditions, particularly the existence of geological structures such as faults and fractures that serve as pathways for hydrothermal fluid migration from depth to the surface [7-8]. Consequently, understanding the flow pathways of hydrothermal fluids constitutes one of the fundamental aspects in the study of geothermal systems [9].

One region with notable geothermal potential in Lampung Province is the Muara Putih Cisarua area, Natar District, South Lampung, which is characterized by the emergence of hot spring manifestations. The geothermal system in this area is considered unique, as its manifestations appear at a considerable distance from active volcanic centers, suggesting that the system is primarily controlled by regional geological structures, particularly the northwest–southeast trending fault system associated with the Lampung-Panjang Fault [10].

The principal geological structure in the study area is the Lampung-Panjang Fault, oriented northwest-southeast (NW-SE), which is known to be tectonically active [11]. The emergence of the Cisarua hot spring is closely associated with this fault system, which acts as the primary migration pathway for hydrothermal fluids ascending from depth to the surface. The occurrence of hot springs at Cisarua is notably distinct from typical geothermal manifestations, which are generally found in proximity to volcanic centers. This locality is situated in a relatively flat terrain and lies at a considerable distance from active volcanism, thus necessitating further investigation to elucidate the mechanisms responsible for hot spring development in this area [12].

From a geological perspective, the Cisarua Hot Spring is located in a lowland environment approximately 16 km from the nearest volcano, Gunung Betung, indicating an absence of direct relationships with volcanic activity [13]. The nearby Merak Batin Natar hot spring manifestation occupies the same geological setting and is controlled by the Lampung-Panjang Fault structural system, demonstrating that both manifestations share a common tectonic rather than volcanic heat source origin.

Based on geological mapping [10], the lithological units in this region comprise several formations of different ages. The oldest unit is the Gunung Kasih Complex (Pzg), consisting of metamorphic rocks including schist, gneiss, quartzite, and marble, interpreted as the regional basement. This unit is intruded by Cretaceous diorite and quartz diorite (Kds) and Cretaceous-Paleogene Branti Granodiorite (Kgdb), which induced contact metamorphism that formed the Marble unit (Pzgm). Overlying the basement is the Pliocene-Pleistocene Lampung Formation (QTl), which is dominated by volcaniclastic deposits including tuffaceous sandstone, conglomerate, and tuffaceous clay interlayered with limestone. The youngest unit is the Holocene Young Volcanic Deposit (Qhvp), consisting of lava flows, volcanic breccia, and tuff with relatively low to moderate consolidation.

A previous study on the geothermal system in the Natar area was conducted by [10]. To investigate fluid flow from a newly drilled well using the geoelectric method to identify hot water flow pathways in the vicinity of the new well hot spring. That study also employed the Very Low Frequency Electromagnetic (VLF-EM) method to detect the presence of fault structures suspected to serve as migration pathways for hydrothermal fluids. The results revealed low resistivity zones interpreted as hot fluid flow pathways potentially associated with local geological structures. Furthermore, the geothermal manifestations in the Natar and Cisarua areas were classified as bicarbonate-type hot springs genetically related to the regional structural system of the Lampung-Panjang Fault [12].

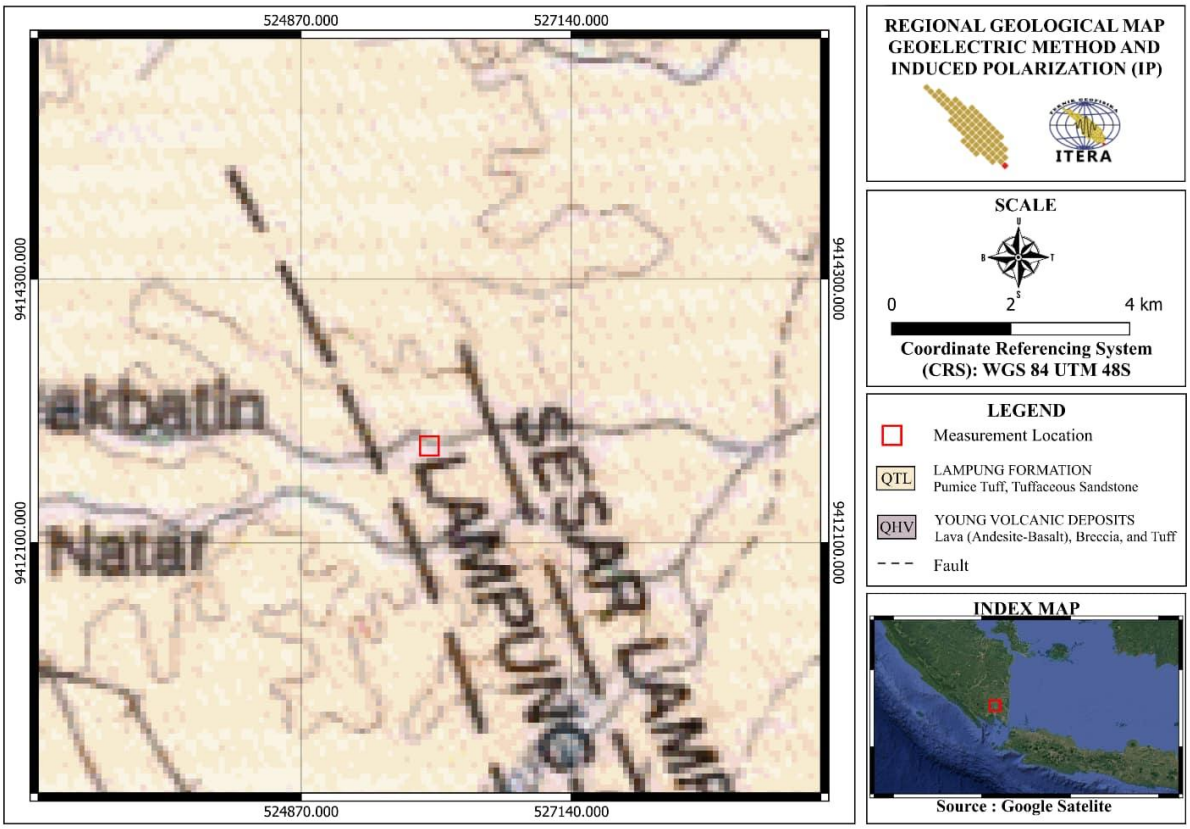

Figure 1. Regional Geological Map

Nevertheless, that study was subject to several limitations. The number of measurement tracks employed was relatively limited, resulting in an investigative coverage that was insufficient to comprehensively characterize the subsurface conditions across the area. In addition, the focus of the previous research was primarily directed toward identifying fluid flow pathways associated with the newly drilled well, while the relationship between fluid flow pathways and the older well within the area had not been examined in detail. These limitations have resulted in an incomplete understanding of the hydrothermal fluid flow distribution pattern within the Cisarua hot spring area.

To address these limitations, this research was undertaken to extend previous investigations by expanding spatial coverage to four measurement profiles and re-analyzing subsurface hydrothermal fluid flow pathways across the broader Cisarua Hot Spring area. Unlike previous studies, this investigation explicitly examines the hydrological relationship between the old well and new well as distinct manifestation points, integrating Electrical Resistivity Tomography (ERT) and Induced Polarization (IP) data from multiple survey lines to construct a three-dimensional (3D) subsurface model. This integrated approach enables more comprehensive characterization of the hydrothermal system architecture and supports more robust decision-making for sustainable geothermal resource development in the region.

2. Research Methods

2.1. Study Area

Administratively, the study area exhibiting geothermal manifestations is the Cisarua Hot Spring, located in Natar District, South Lampung Regency, Lampung Province. Geographically, the site is situated approximately 4 km to the east of Natar Town and approximately 15 km to the north of

Bandar Lampung City. The occurrence of hot spring discharge in this area is presumed to be associated with regional geological structural activity, particularly the Lampung-Panjang Fault trending northwest-southeast (NW-SE) [11].

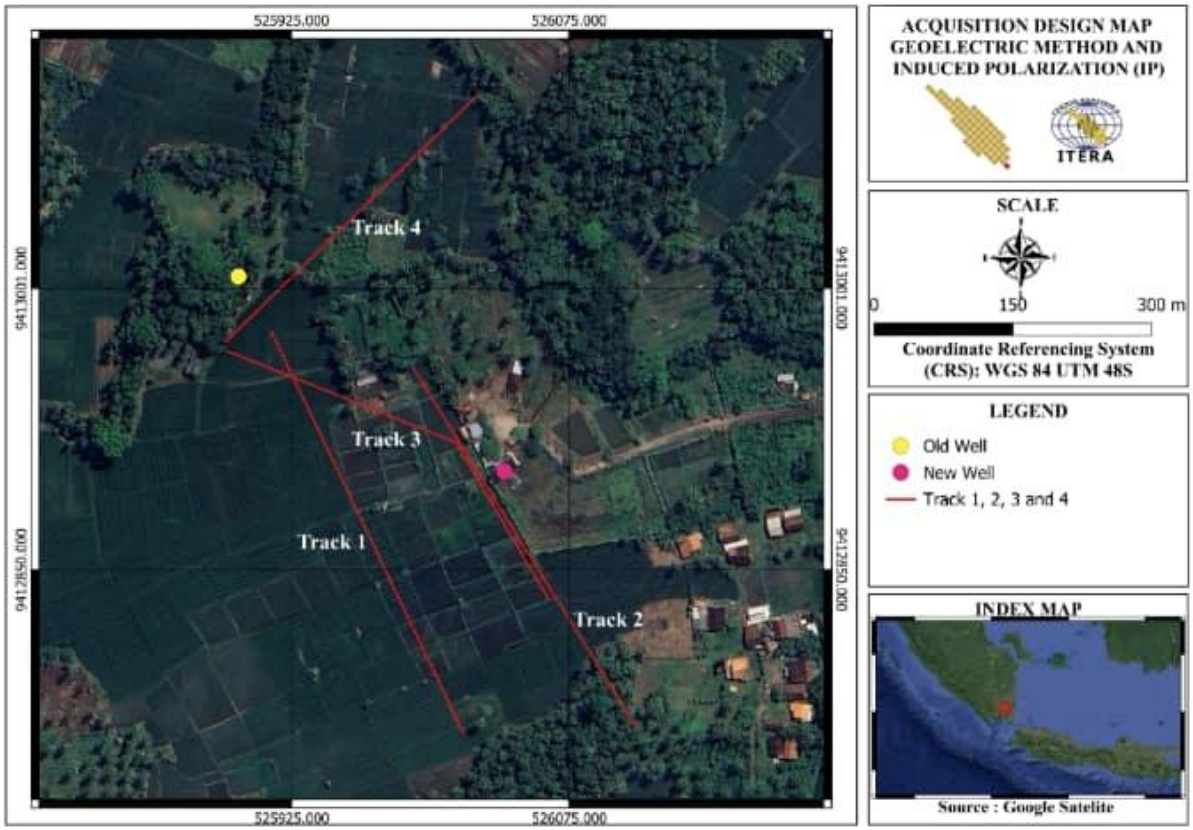

Figure 2. Acquisition Design Map

2.2. Research Parameters

This study employed two geophysical methods, as described below:

2.2.1. Geoelectric Method

The working principle of the geoelectric method involves injecting an electric current into the ground surface through a pair of current electrodes and measuring the resulting potential difference using a separate pair of potential electrodes [14-15]. When an electric current is injected into a medium and the potential difference (voltage) is measured, the resistivity value of the medium can be estimated [16-17]. Field data acquisition was conducted using an ARES (Automatic Resistivity Equipment System) instrument along four measurement profiles.

Each profile was 235 m in length with an electrode spacing of 5 m, achieving maximum investigation depths of approximately 44.65 m. A total of 48 electrodes were linearly deployed along each survey line to obtain subsurface resistivity data. The acquired data were subsequently processed using RES2DINV software through least-squares inversion to generate two-dimensional resistivity distribution models representing the subsurface conditions within the study area [18]. The geoelectric resistivity method is based on Ohm's Law, expressed by the following equation [19]:

$$R = \rho \frac{L}{A} \quad (1)$$

The resistivity values measured by this method do not represent true resistivity, but rather apparent resistivity [20].

$$\rho_a = \frac{K\Delta V}{I} \quad (2)$$

The electrode configuration employed in this study is the Wenner-Schlumberger configuration. This configuration operates on a constant spacing system, where the factor *n* is defined as the ratio of the distance between electrodes C1-P1 (or C2-P2) to the spacing between P1-P2 [21-23]. If the spacing between the potential electrodes (P1 and P2) is *a*, then the distance between the current electrodes (C1 and C2) is $2na + a$ [24-25]. The resistivity determination process utilizes four electrodes arranged in a collinear configuration [26-27].

2.2.2. Induced Polarization Method

The Induced Polarization (IP) method measures the degree of polarization within rocks as a result of an electric current passing through them [28-31]. The fundamental principle underlying the induced polarization phenomenon is the flow of current that generates a charge transfer reaction between electrolytic ions and minerals exhibiting a high degree of polarizability [32-35]. The Induced Polarization (IP) method operates by measuring the polarization effect occurring within a medium in response to an applied electric current [36-39]. The electric current is injected into the ground through two current electrodes (C1 and C2), after which the current passes through a capacitor and is received by two potential electrodes (P1 and P2) [40-41]. When the electric current is terminated, the potential difference should theoretically return to zero. In practice, however, the potential difference does not instantaneously reach zero; instead, it decays gradually toward zero. This phenomenon is known as the overvoltage effect [42].

The acquired data were further processed using RES2DINV software via least-squares inversion algorithm to produce two-dimensional chargeability and resistivity. These chargeability sections were employed to identify zones of hydrothermal alteration and accumulation of polarizable minerals within the subsurface. The integration of resistivity and chargeability parameters enabled comprehensive characterization of the subsurface geothermal architecture and differentiation between clay cap, reservoir, and host rock lithologies.

The Induced Polarization method, when applied in the time domain, involves the use of direct current (DC) injected at different time intervals. To determine the chargeability value (*M*), the secondary voltage (*Vs*) measured after the current is switched off is compared to the primary voltage (*Vp*). If the decay curve is sampled at several points, the values of the integral are effectively a measure of the potential existing at different times, that is, V(t 1), V(t 2),… V(tn) [43]. This is an extension of the measurement from which one also obtains the decay curve shape [44].

This is defined as [45]:

$$M = \frac{1}{V_C}\int_{t_1}^{t_2} V(t)\, dt \quad (3)$$

and is the most commonly used quantity in time-domain Induced Polarization (IP) measurement. When V(t) and V_c have the same units, the chargeability M is in milliseconds [45-46].

2.3 Research Workflow

The research workflow commenced with a preparatory stage encompassing field geological observations, literature review, and regional geological map analysis. Field observations were conducted to directly identify surface geological characteristics, including the presence of geothermal manifestations and indications of geological structures such as faults and fractures that potentially control the hydrothermal system. The literature review served to establish a robust theoretical framework while simultaneously evaluating methodological approaches employed in previous studies. Regional geological map analysis was utilized to comprehend the configuration of geological structures at a broader scale and their role in controlling the distribution of the geothermal system within the study area.

The subsequent stage involved the design of a data acquisition scheme, with particular emphasis on determining the position and orientation of measurement lines. This design was conducted systematically while considering local geological conditions and research objectives, specifically to capture subsurface indications of hydrothermal fluid flow pathways. The measurement lines were oriented in a northwest-southeast direction to maximize the detection of structural features associated with the Lampung–Panjang Fault, thereby maximizing the potential to detect lateral and vertical variations in subsurface physical properties along the structural corridor controlling hydrothermal fluid migration. The position of each line was determined through integration of surface manifestation distribution data and structural geological information obtained during the preparatory stage, ensuring that data acquisition adequately represented the geothermal system target zone and captured spatial relationships between the old well and new well manifestation points.

Data acquisition was performed using the geoelectric and Induced Polarization (IP) methods along the predesigned tracks. Measurements were conducted systematically to obtain resistivity and chargeability values across all designated survey lines. The resistivity parameter was utilized to identify variations in fluid distribution based on contrasts in electrical conductivity among different rock and fluid types, whereas chargeability was employed to characterize the polarization response of rocks, which is generally associated with alteration processes and the presence of specific minerals within the hydrothermal system. The acquired data were subsequently processed and inverted using two-dimensional (2D) inversion software to generate subsurface resistivity and chargeability cross-sections, which served as the primary basis for interpreting the geometry and distribution of the hydrothermal system in the study area [47].

The acquired data were subsequently processed to improve data quality, primarily by minimizing the influence of noise that may have been introduced during the acquisition process. Following this, an inversion procedure was applied to transform the field data into a subsurface model. Upon completion of the processing stage, an iterative data inversion procedure was carried out to transform the measured data into a subsurface model that quantitatively represents the distribution of resistivity and chargeability. The inversion process was performed until a stable model was achieved with an acceptable level of error. The inversion results were then visualized as two-dimensional (2D) cross-sections depicting the variation of parameter values with respect to depth and lateral position [48].

Data from multiple measurement tracks were systematically integrated to construct a simplified three-dimensional (3D) model of the subsurface geothermal system. This 3D visualization approach provides a more comprehensive spatial representation compared to conventional 2D cross-sectional analysis, thereby facilitating a more thorough understanding of the geometric relationships and spatial continuity of anomalous zones throughout the study area. The 3D model was developed by correlating resistivity and chargeability distributions across all four measurement tracks, enabling the identification of anomalous features that extend laterally and vertically in three dimensions. This spatial integration approach is particularly instrumental in revealing the three-dimensional architecture of the hydrothermal system and its spatial association with the prevailing regional geological structures, such as fault zones and lithological contacts. Furthermore, the 3D model enables a more detailed analysis of the continuity and interconnection of hydrothermal fluid flow pathways between distinct manifestation points, as well as elucidating the subsurface geometry of the clay cap and reservoir zones. This methodology provides enhanced capability for conceptualizing the overall geometry and subsurface characteristics of the non-volcanic geothermal system.

The final analytical stage consisted of comprehensive data interpretation, carried out through systematic correlation of the 3D modeling results with the prevailing geological and structural conditions documented in the study area. Through this integrated interpretation process, hydrothermal fluid flow patterns and their spatial relationship with the geological structures (particularly the Lampung-Panjang Fault) were identified and characterized. The interpretation incorporated available geological information, including lithological boundaries, structural lineaments, and surface manifestation locations, to validate the geophysical findings and enhance the

reliability of the conclusions. Additionally, the interpretation specifically addressed the interrelationship between the two distinct manifestation sources namely the old well and the new well by examining their spatial proximity, anomalous characteristics (resistivity and chargeability signatures), and connectivity patterns. This comprehensive analysis provided evidence that both manifestation points represent components of a single, internally connected, and fault-controlled hydrothermal system, rather than isolated geothermal features. The integrated approach thus enabled a more robust understanding of the subsurface geothermal architecture and the mechanisms governing fluid circulation in this non-volcanic setting.

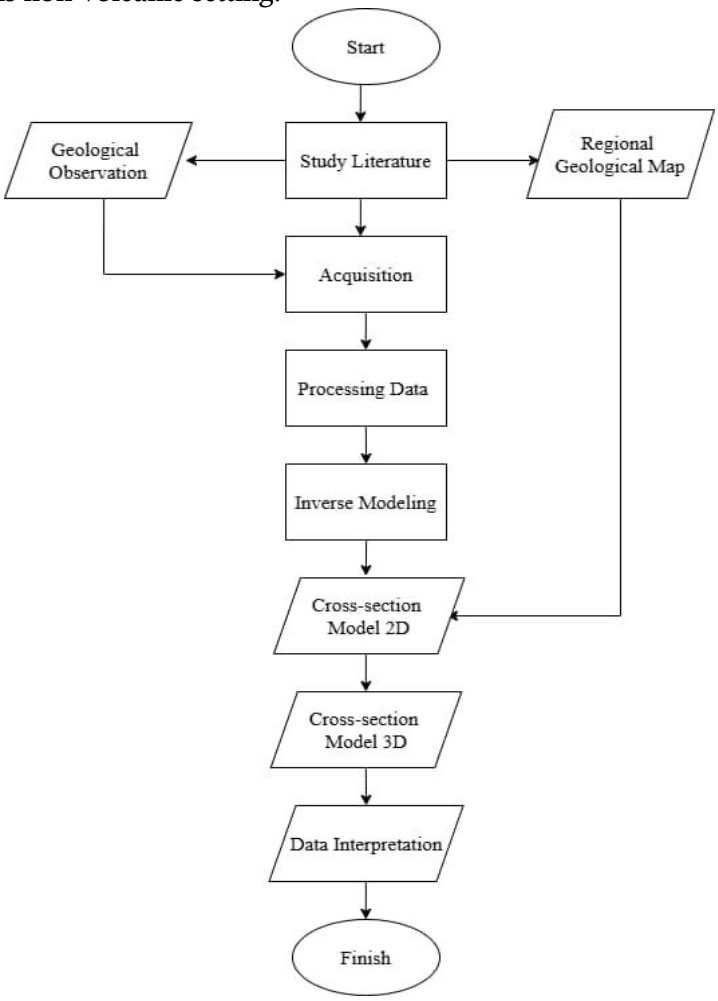

Figure 1. Research Workflow

3. Results and Discussion

Field data from Electrical Resistivity Tomography (ERT) and Induced Polarization (IP) measurements. The inversion results are presented in the form of 2D and 3D cross-sections illustrating the distribution of resistivity (Ωm) and chargeability (ms) values with depth for subsequent geological interpretation. The interpretation of resistivity values refers to previous studies that have been correlated with local geological conditions [10], [49]. While the interpretation of chargeability values refers to the classifications by Telford (1976) [45] and Muhamad Zainul Muhlisin (2019) [50], which correlate chargeability ranges with lithological types.

Table 1. Resistivity reference

Previous Studies	Rock Type	Resistivity Values (Ωm)
(Atsani et al., 2026) [10]	Tuff Clay	0–20
	Sandy Clay	20–70
(Rizka, 2019) [49]	Tuff Clay	< 20
	Tuff Sand	20 – 80

Table 2. Chargeability Reference by Telford (1976)[45] and Muhamad Zainul Muhlisin (2019)[50]

Chargeability Values	Rock Type
20 – 35 ms	Clay

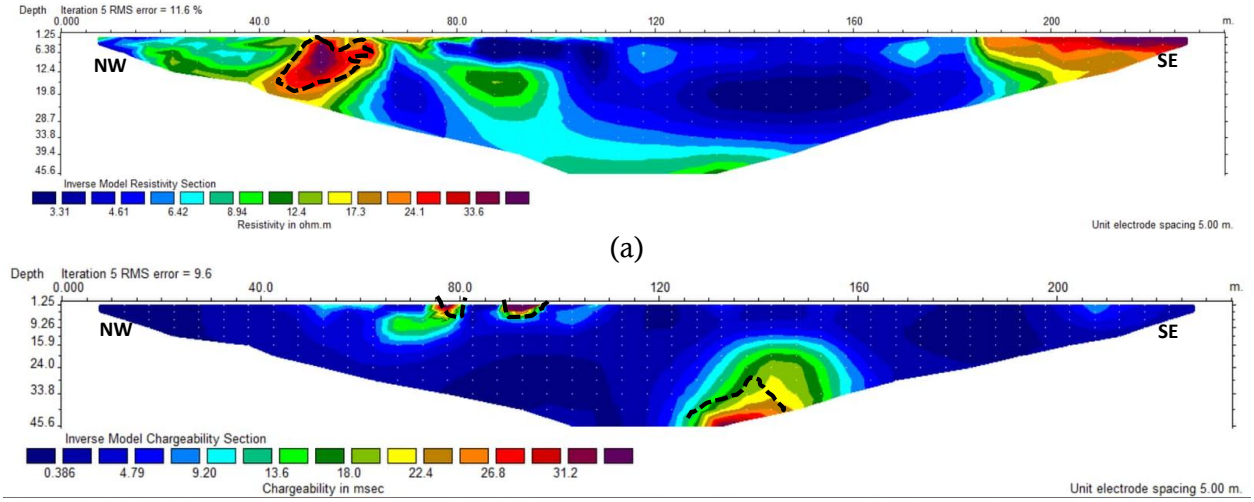

Figure 2. Electrical Resistivity Tomography (ERT) cross-sections along Traverse 1: (a) Geoelectric cross-section, (b) Induced Polarization (IP) cross-section

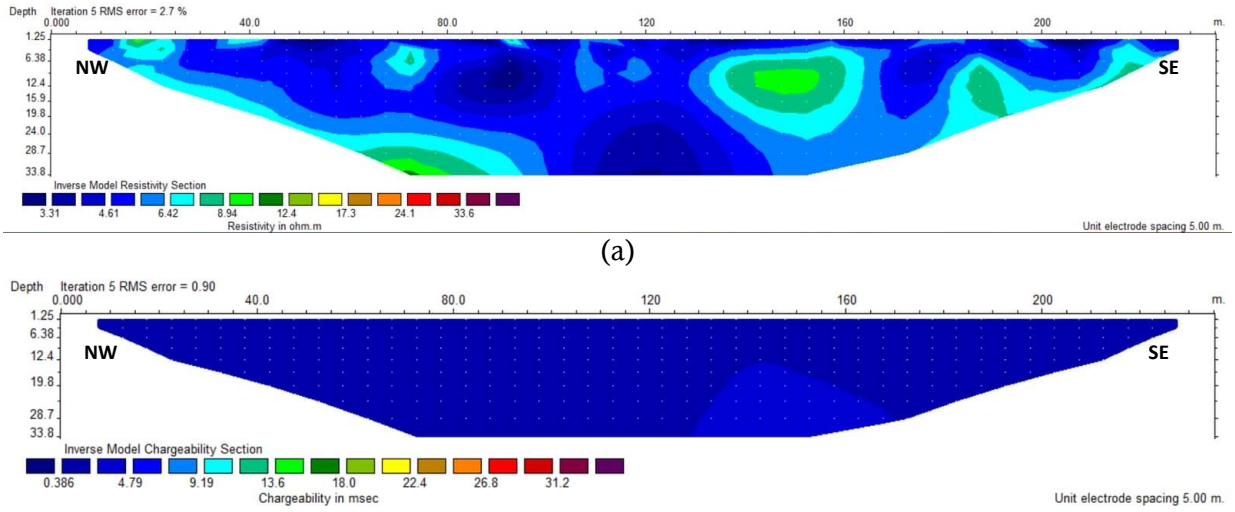

Figure 3. Electrical Resistivity Tomography (ERT) cross-sections along Traverse 2: (a) Geoelectric cross-section, (b) Induced Polarization (IP) cross-section

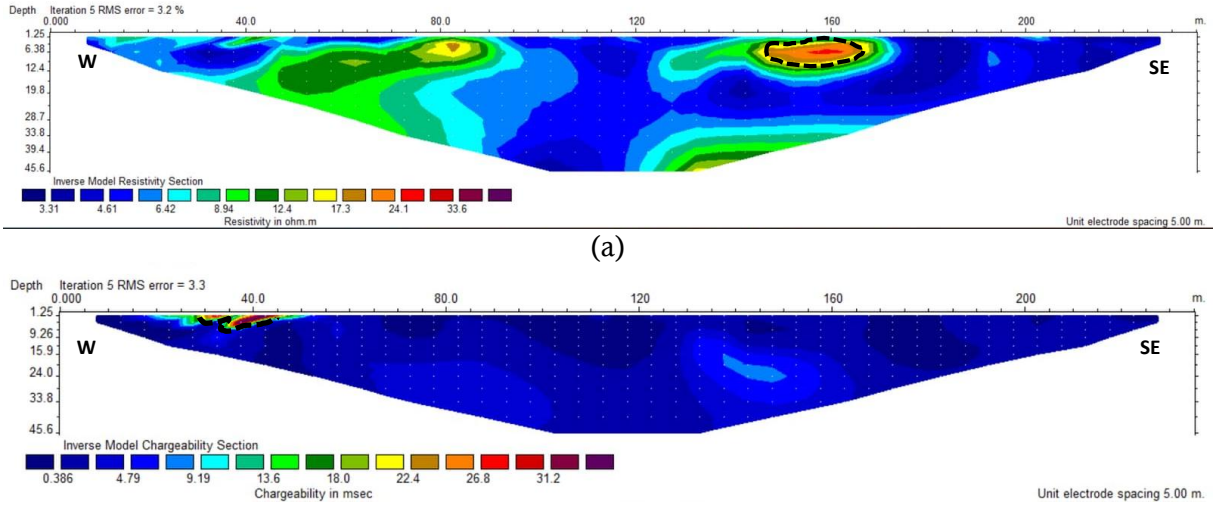

Figure 4. Electrical Resistivity Tomography (ERT) cross-sections along Traverse 3: (a) Geoelectric cross-section, (b) Induced Polarization (IP) cross-section

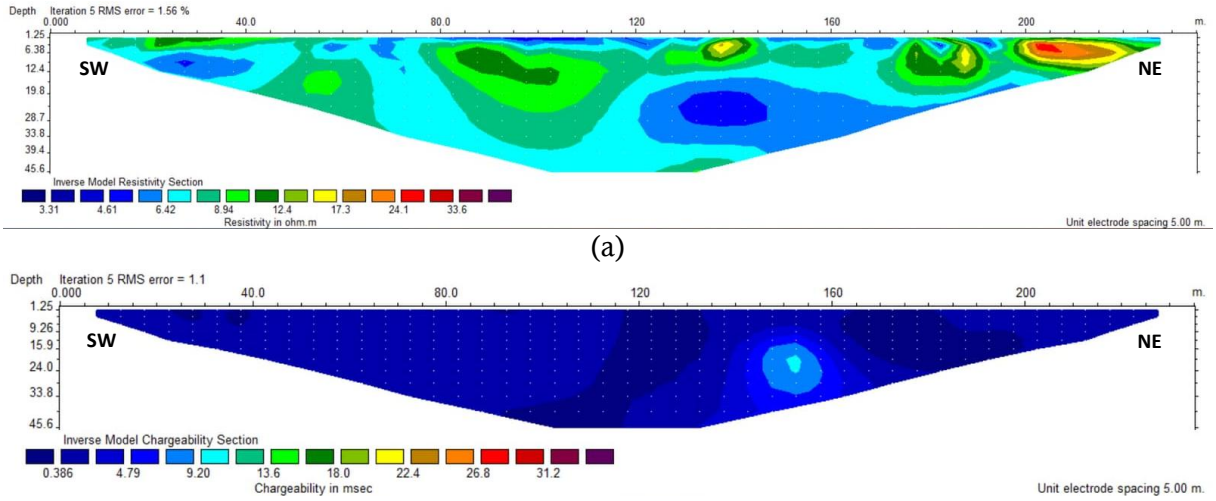

Figure 5. Electrical Resistivity Tomography (ERT) cross-sections along Traverse 4: (a) Geoelectric cross-section, (b) Induced Polarization (IP) cross-section

The inversion process for geophysical resistivity and Induced Polarization (IP) data was performed using a least-squares inversion approach, which minimizes the difference between the field measurement data and the model response. In this study, the inversion was performed for up to 5 iterations on each profile. Each iteration gradually refines the subsurface model until a relatively small root mean square error (RMS error) is obtained (0.9%-11.6%) [51-52].

Table 1. RMS error of 2D resistivity and IP inversion results per survey track

Survey Track	Error Res (%)	Error IP (%)	Iteration
1	11.6	9.6	5
2	2.7	0.90	5
3	3.2	0.90	5
4	3.5	1.20	5

The relatively higher error rates on Track 1 (11.6% for resistivity and 9.6% for Induced Polarization) are believed to be related to a degradation in data acquisition quality toward the end of the line due to a decrease in the instrument's power source, which affected the stability of electrical current injection at electrodes located farther from the starting point of the measurement. This condition caused a sharp increase in data at several observation points, resulting in higher error values compared to other lines. Nevertheless, these error values remain within an acceptable range for geological interpretation and do not affect the main anomaly patterns identified in the inversion cross-section.

The inversion results show a resistivity range of 3.3-33.6 Ωm. According to the reference [10], this range correlates with lithologies ranging from tuffaceous clay (low resistivity, <20 Ωm) to tuffaceous sand (medium resistivity, 20-70 Ωm). Low resistivity values are interpreted as conductive materials that are generally fluid-saturated, while medium resistivity reflects more permeable materials [3]. The chargeability parameter from the Induced Polarization (IP) method indicates the rock's polarizability response, which generally increases in zones containing dissolved minerals or ionically charged fluids.

The correlation between resistivity and chargeability indicates that zones with low to medium resistivity associated with high chargeability are a primary indication of fluid pathways. On Profile 1, the resistivity cross-section shows a dominance of conductive zones in the central part of the profile, which correlates with high chargeability anomalies in the Induced Polarization (IP) cross-section. In Figure 4, the correlation pattern between low resistivity and high chargeability on Profile 1 indicates the presence of an active hydrothermal fluid flow path that is structurally connected to the surface, a finding reinforced by its proximity to the hot water manifestation point, as shown on the acquisition design map in Figure 2[52].

Track 2 shows a relatively homogeneous distribution of low resistivity with low to moderate chargeability values. These conditions indicate the dominance of water-saturated tuffaceous clay lithology without the presence of focused fluid pathways. In Track 3, a zone of medium resistivity was identified, flanked by low resistivity and correlated with increased chargeability. In Figure 6, this zone is interpreted as a more permeable tuff sand layer that functions as a fluid flow path. Meanwhile, Profile 4 shows variations in resistivity that are not accompanied by corresponding changes in chargeability, suggesting that changes in physical properties are more controlled by lithological variations than by the presence of charged fluid.

In the Induced Polarization (IP) cross-section, particularly in Profiles 1 and 3, zones with high chargeability values (>20 ms) that coincide with low to medium resistivity are interpreted as clay layers that have undergone hydrothermal alteration [29]. These layers act as cap rocks low permeability layers that seal the upper part of the hot fluid reservoir. The presence of cap rocks is crucial because these layers prevent the fluid from easily escaping to the surface in a diffuse manner, thereby maintaining the thermal gradient and pressure within the reservoir.

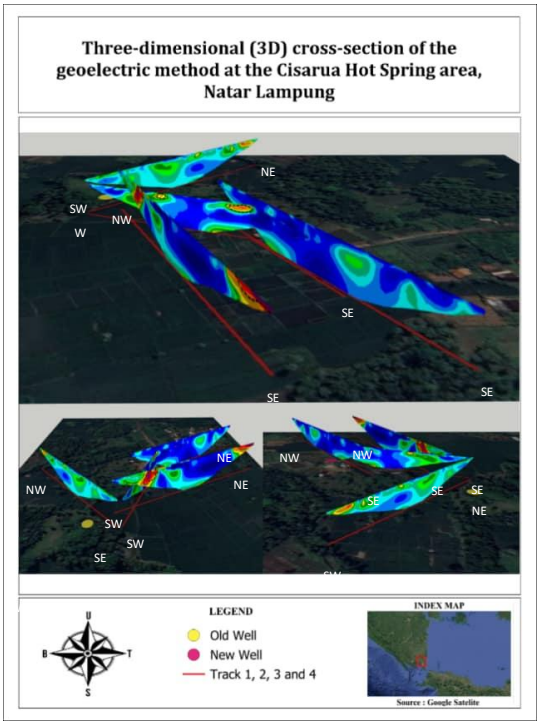

Figure 6. Three-dimensional (3D) cross-section of the geoelectric method at the Cisarua Hot Spring area, Natar, Lampung

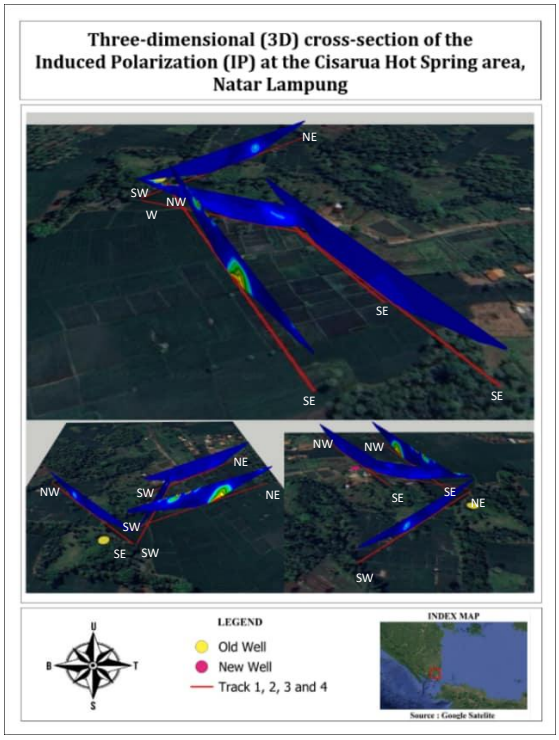

Figure 9. Three-dimensional (3D) cross-section of the Induced Polarization (IP) at the Cisarua Hot Spring area, Natar, Lampung

This interpretation is consistent with the regional geological conditions of the study area, which is part of the Lampung Formation, composed of tuffaceous clay, tuffaceous sand, and clay. This is reflected in the distribution of resistivity and chargeability, which tend to align with the orientation of these structures. The identified zones, particularly along track 1 and 3, exhibit low to moderate resistivity characteristics associated with relatively high chargeability, and are therefore interpreted as fluid pathways.

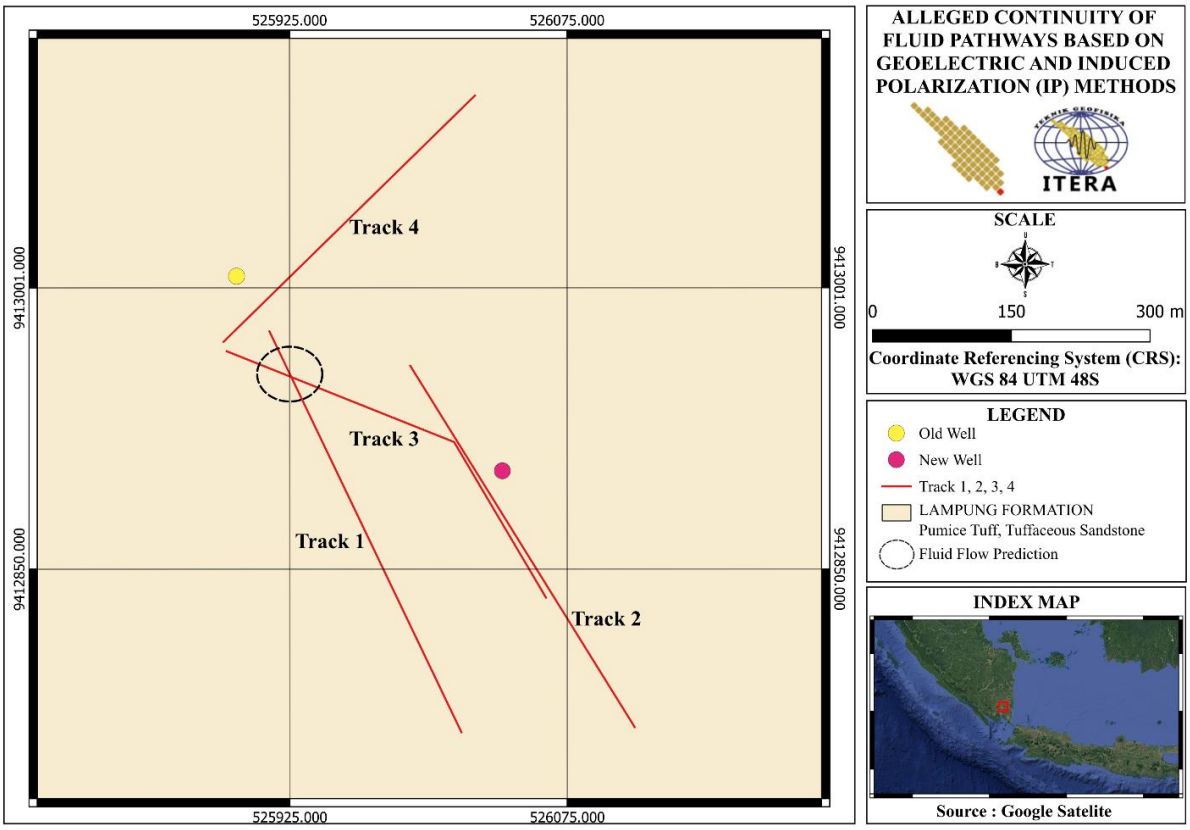

Figure 7. Fluid Flow Prediction Map

Based on the interpretation of the four survey tracks, anomaly zones are marked with dashed circles or the notation "fluid flow prediction," which indicates the estimated flow of hot fluid zones. The orientation of the survey tracks indicates that track 1 and track 3 extend in a northwest–southeast (NW–SE) direction [11].

These zones are interpreted as areas with interconnected subsurface anomalies and are suspected to represent pathways of hydrothermal fluid flow continuity. This interpretation is based on the correlation between low to moderate resistivity values and relatively high chargeability values, indicating the presence of permeable zones filled with hot fluid and influenced by hydrothermal alteration processes [9]. The presence of this predicted fluid flow zone indicates that the subsurface fluid system in the study area is continuously interconnected, following the control of regional geological structures. When linked to the surface distribution of hot water, both in old and new wells, the fluid flow prediction of this zone reveals a connectivity pattern pointing to a single, unified fluid flow system.

This indicates that the zone has the potential to serve as a primary migration pathway for hot fluids from the reservoir to the surface. Thus, the area marked as a fluid flow prediction zone is interpreted as a potential zone for the accumulation of subsurface hot fluids. If drilling is conducted in this zone, there is a possibility of discovering new hot fluid discharge points associated with the

geological conditions and the presence of hot water manifestations that follow the direction of the main structural trend in the study area. Based on the integration of inversion results, acquisition design maps, and regional geology, the direction of fluid flow in the Cisarua Hot Springs area is interpreted to follow the direction of the main Lampung-Panjang Fault structure, namely from the northwest-southeast (NW-SE), as shown in Figure 1. This interpretation is supported by the alignment of hot spring manifestations (old and new wells) along this direction [10-11].

4. Conclusion

The application of Electrical Resistivity Tomography (ERT) and Induced Polarization (IP) methods to four trajectories in the Cisarua Hot Springs area identified two main lithologies: tuffaceous clay (resistivity <20 Ωm) and tuffaceous sand (20–33.6 Ωm), consistent with the characteristics of the Lampung Formation. The RMS error ranged from 0.9% to 11.6%, confirming the inversion model for geological interpretation. The low-resistivity zone associated with high chargeability (>20 ms) in Trajectories 1 and 3 is interpreted as an active hydrothermal fluid flow pathway controlled by the northwest southeast trending Lampung Panjang Fault. The altered clay layer identified above this zone serves as a reservoir cap, maintaining the pressure system and thermal gradient.

The anomalous continuity in Trajectories 1 and 3 demonstrates that the old and new wells are part of a single, interconnected hydrothermal system. Subsurface fluid migration is controlled by the Lampung–Panjang Fault, which serves as the primary pathway for hot fluid movement to the surface. These findings provide a scientific basis for further geothermal exploration in the South Lampung region.

References

[1] A. A. Safitri, E. F. Andaresta, And D. A. Suaidi. (2022). Identifikasi Lapisan Hidrotermal Dengan Menggunakan Metode Geolistrik Resistivitas Konfigurasi Wenner (Studi Kasus Wilayah Panas Bumi Cangar), *J. Mipa Dan Pembelajarannya*, Vol. 2, No. 4, Pp. 291–299.

[2] Putri, U. A., Paembonan, A. Y., Antosia, R. M., & Irawati, S. M. (2024). Analisis Metode Geolistrik 2D dan VLF-EM untuk Mendeteksi Jalur Air Panas Desa Jatimulyo, Kecamatan Jati Agung, Kabupaten Lampung Selatan. *Jurnal Geosains dan Teknologi*, *7*(1), 9-18.

[3] Jones, D. J., Randles, T., Kearsey, T., Pharaoh, T. C., & Newell, A. (2023). Deep geothermal resource assessment of early carboniferous limestones for Central and Southern Great Britain. *Geothermics*, *109*, 102649.

[4] Octavani, A. S., & Kadri, M. (2018). Analisis Resistivitas Bawah Permukaan Menggunakan Metode Geolistrik Konfigurasi Wenner–Schlumberger Dan Dipole-Dipole Di Daerah Geothermal Gunung Sibayak Kabupaten Karo Provinsi Sumatera Utara. *Jurnal Einstein*.

[5] Fariña-González, D., García-Afonso, Ó., & Delgado-Torres, A. M. (2025). Assessment of geothermal resources for power generation on La Palma Island, Canary Islands. *Geothermics*, *127*, 103263.

[6] Bandara, D., Smit, J., Christiansen, R. O., Subasinghe, D., Wohnlich, S., & Heinze, T. (2024). Enhancing the hot water yield in low enthalpy geothermal systems in Sri Lanka. *Renewable Energy*, *235*, 121386.

[7] Betancourt, C., Morata, D., Vidal, J., & Maza, S. (2025). Hydrothermal alteration in the geothermal system of the Irruputuncu volcano deep wells PGC-01 and PGC-02, Northern Chile. *Geothermal Energy*, *13*(1), 29.

[8] Zhai, D., Wu, J., Zhao, Q., Voudouris, P., Tombros, S., Wang, X., ... & Liu, J. (2025). Alteration and metallogenic zonation in magmatic-hydrothermal ore systems: scientific understandings and exploration implications. *Journal of Earth Science*, *36*(3), 1303-1308.

[9] Yang, Y., Zhang, J., Wang, X., Liang, M., Li, D., Liang, M., ... & Li, X. (2024). Deep structure

and geothermal resource effects of the Gonghe basin revealed by 3D magnetotelluric. *Geothermal Energy*, *12*(1), 6.

[10] Atsani, A. R., Rumansah, R. P. P., Saragi, I. U., Cahyanto, M. H., & Irawati, S. M. (2026). Identifikasi Jalur Air Panas dengan Menggunakan Metode Geolistrik 2D dan Very Low Frequency Electromagnetic di Desa Muara Putih, Kecamatan Natar, Lampung Selatan. *Jurnal Geosains dan Teknologi*.

[11] Suharno, S., Aritonang, R. B., Ahmad, Z., & Rustadi, R. (2012, November). Sistem Panas Bumi Cisarua Natar Lampung Selatan. In *Proceedings The 12TH Annual Indonesian Geothermal Association Meeting & Conference*. Asosiasi Panas Bumi Indonesia.

[12] Juliarka, B. R., & Iqbal, M. (2020). Model Gaya Berat 2D untuk mengungkap Struktur Geologi Bawah Permukaan Pada Daerah Panas Bumi Natar. *Buletin Sumber Daya Geologi*, *15*(1), 39-49.

[13] Santoso, N. A., Junian, W. E., Ramayanti, F., Rizki, R., & Alawiyah, S. (2025). Multimethod Approach To The Study Of Subsurface In Merak Batin Hot Spring, Natar, Lampung. *Jurnal Geosaintek*, *11*(1), 63-71.

[14] Blanchy, G., Saneiyan, S., Boyd, J., McLachlan, P., & Binley, A. (2020). ResIPy, an intuitive open source software for complex geoelectrical inversion/modeling. *Computers & Geosciences*, *137*, 104423.

[15] Tso, C. H. M., Iglesias, M., Wilkinson, P., Kuras, O., Chambers, J., & Binley, A. (2021). Efficient multiscale imaging of subsurface resistivity with uncertainty quantification using ensemble Kalman inversion. *Geophysical Journal International*, *225*(2), 887-905.

[16] Winarni, A. (2015). Aplikasi Metode Geolistrik Resistivitas Konfigurasi Wenner Untuk Menentukan Struktur Tanah di Halaman Belakang SCC ITS Surabaya (Halaman 1 sd 5). *Jurnal Fisika Indonesia*.

[17] Alam, M. J. B., Ahmed, A., & Alam, M. Z. (2024). Application of electrical resistivity tomography in geotechnical and geoenvironmental engineering aspect. *Geotechnics*, *4*(2), 399-414.

[18] Singh, S., Gautam, P. K., Bagchi, D., Singh, S., Kumar, S., & Kannaujiya, S. (2021). 2D Electrical resistivity imaging for geothermal groundwater characterization and rejuvenation of the Gaurikund hot spring in the Main Central Thrust (MCT) zone of the Garhwal Himalaya, Uttrakhand, India. *Groundwater for Sustainable Development*, *15*, 100686.

[19] Telford, W. M., Geldart, L. P., & Sheriff, R. E. (1990). *Applied geophysics*. Cambridge university press.

[20] R. Wilyan Pratama. (2019). Aplikasi Metode Geolistrik Resistivitas Konfigurasi Wenner-Schlumberger Untuk Mengidentifikasi Provinsi Lampung, *J. Geofis. Eksplor. Vol.*, Vol. 5, No. 1, Pp. 30–44.

[21] Aminulloh, D., Ekasara, A. R., & Adha, I. (2025). Analisa Komposisi Material Bawah Tanah Hasil Letusan Gunung Merapi di Dusun Mliwis, Kecamatan Cepogo, Boyolali dengan Metode Geolistrik Resistivitas Konfigurasi Wenner Schlumberger. *Jurnal Ilmiah Geomatika*, *5*(1), 25-33.

[22] Singh, U., & Sharma, P. K. (2022). Study on geometric factor and sensitivity of subsurface for different electrical resistivity Tomography Arrays. *Arabian Journal of Geosciences*, *15*(7), 560.

[23] AL-Hameedawi, M. M., Thabit, J. M., & AL-Menshed, F. H. (2021). Some notes about three types of inhomogeneity and their effect on the electrical resistivity tomography data. *Journal of Applied Geophysics*, *191*, 104360.

[24] Anas, N. A., Syamsuddin, S., Harimei, B., & Nasri, M. (2020). Identifikasi Struktur Bawah Permukaan Di Sekitar Manifestasi Panasbumi Reatoa Kabupaten Maros Menggunakan Survey Geolistrik Resistivitas. *Jurnal Geocelebes*, *4*(1), 23-32.

[25] Yan, J., Zeng, Z., Zhao, X., An, B., Bai, L., Zhao, J., & Li, J. (2023). A new electrical resistivity tomography scheme of borehole-to-surface-to-cliff detection and imaging for grotto rock structure. *Remote Sensing*, *15*(2), 311.

[26] Utiya, J., As'ari, A. A., & Tongkukut, S. H. (2015). Metode geolistrik restivitas konfigurasi Wenner-Schlumberger dan konfigurasi dipole-dipole untuk identifikasi Patahan Manado di Kecamatan Paaldua Kota Manado. *Jurnal Ilmiah Sains*, *15*(2), 135-141.

[27] Sáez Blázquez, C., Martín Nieto, I., Carrasco, J., Carrasco, P., Porras, D., Maté-González, M. Á., ... & González-Aguilera, D. (2024). Applying deep electrical-resistivity tomography techniques for the exploration of medium-and low-geothermal energy resources. *Energies*, *17*(8), 1836.

[28] Yuniarto, A. H. P. (2020). Metode Induced Polarization Dan Resistivitas Dalam Eksplorasi Emas Di Blok "Cpy" Gunung Pongkor Kabupaten Bogor. *Jurnal Geosaintek*, *6*(3), 117-126.

[29] Piolat, L., Géraud, Y., & Revil, A. (2023). Induced polarization images the plumbing system of hydrothermal vents in an intracontinental rift, Lake Abhé, Republic of Djibouti. *Geophysical Research Letters*, *50*(24), e2023GL105145.

[30] Ali, M. A. H., Mewafy, F. M., Qian, W., Alshehri, F., Ahmed, M. S., & Saleem, H. A. (2023). Integration of electrical resistivity tomography and induced polarization for characterization and mapping of (Pb-Zn-Ag) sulfide deposits. *Minerals*, *13*(7), 986.

[31] Cox, Leif H., Michael S. Zhdanov, and Alexander Prikhodko. "Inversion for 3D Conductivity and Chargeability Models Using EM Data Acquired by the New Airborne TargetEM System in Ontario, Canada." *Minerals* 14.3 (2024): 237.

[32] Umar, E. P. (2020). Identifikasi Zona Mineralisasi Emas Menggunakan Metode Resistivitas Dan Induksi Polarisasi (Ip) di Desa Lintidu Kabupaten Buol. *Jurnal Geocelebes*, *4*(2), 144-149.

[33] Kim, B., Deparis, J., Bretaudeau, F., Vedrine, S., Kamm, J., Autio, U., ... & Darnet, M. (2026). Three-dimensional geoelectrical imaging beyond 1 km depth for mineral exploration: framework of deep electrical resistivity tomography and induced polarization with advanced strategies. *Geophysical Journal International*, *244*(3), ggaf460.

[34] Qi, Y., & Wu, Y. (2025). Revisiting the relationship between induced polarization and surface conductivity: Ratios from laboratory to field. *Journal of Geophysical Research: Solid Earth*, *130*(4), e2024JB030406.

[35] Liu, Y., Heinson, G., Kay, B., Boren, G., Carter, S., Olivier, G., ... & McAllister, L. (2024). Natural source-field induced polarisation exploration of an iron-oxide copper-gold (IOCG) deposit under thick cover. *Exploration Geophysics*, *55*(6), 657-666.

[36] Harjo, B., Agung, T., Bahri, A. S., & Utama, W. (2017). *Identifikasi Zona Alterasi Hidrotermal Songgoriti Batu Menggunakan Metode Time Domain Induced Polarization (TDIP)* (Doctoral dissertation, Sepuluh Nopember Institute of Technology).

[37] Chen, J., Dauti, F., Wertich, V., Viezzoli, A., Zhang, B., & Fiandaca, G. (2026). 3-D EM inversion considering induced polarization effect. *Geophysical Journal International*, *244*(1), ggaf462.

[38] Munko-Abo, Y., & Zakari, A. (2025). The use of electrical resistivity imaging and induced polarization surveys to investigate underground tunnels filled with water, case study—Akoon, Tarkwa-Ghana. *Journal of Umm Al-Qura University for Engineering and Architecture*, *16*(2), 370-378.

[39] Macnae, J. (2025). A physical interpretation of Cole–Cole equations and their ambiguous time constants for induced polarization models. *Geophysical Journal International*, *243*(2), ggaf362.

[40] Yang, Y., Zhang, G., Yao, C., Deng, Z., Ren, Z., & Li, C. (2023). Application of induced polarization method in mineral resource exploration. *Sustainability*, *15*(4), 3840.

[41] Revil, A., Ghorbani, A., Zhao, X., Mouyeaux, A., Barrère, L., Richard, J., ... & Vaudelet, P. (2024). Groundwater flow paths using combined self-potential, electrical resistivity, and induced polarization signals. *Geophysical Journal International*, *239*(2), 798-820.

[42] Suwiryo, K., Zulfian, Z., & Muhardi, M. (2025). Penerapan Metode Induced Polarization

Untuk Mengidentifikasi Sebaran Air Asin di Daerah Sekitar Sumur Garam Desa Manis Raya. *JIIF (Jurnal Ilmu dan Inovasi Fisika)*, *9*(1), 24-33.

[43] Su, Z., Revil, A., Ghorbani, A., Zhang, X., Zhao, X., & Richard, J. (2023). Combining electrical resistivity, induced polarization, and self-potential for a better detection of ore bodies. *Minerals*, *14*(1), 12.

[44] Hase, J., Gurin, G., Titov, K., & Kemna, A. (2023). Conversion of induced polarization data and their uncertainty from time domain to frequency domain using debye decomposition. *Minerals*, *13*(7), 955.

[45] Telford, W. M., Geldart, L. P., & Sheriff, R. E. (1990). *Applied geophysics*. Cambridge university press.

[46] Pertiwi, P., & Jiwandono, T. W. (2021). Analisis Data Resistivitas Dan Polarisasi Terimbas Guna Mendeteksi Keberadaan Mineralisasi Daerah Karangsambung. *JGE (Jurnal Geofisika Eksplorasi)*, *7*(1), 71-83.

[47] Adel, S., Ardeshir, H., & Aref, S. (2022). Geophysical explorations by resistivity and induced polarization methods for the copper deposit, South Khorasan, Iran. *Известия Томского политехнического университета. Инжиниринг георесурсов*, *333*(3), 99-110.

[48] Rahmayani, A. (2020). *Identifikasi Pola Penyebaran Fluida Bawah Permukaan Daerah Geothermal Menggunakan Geolistrik Di Daerah Sorik Marapi Kabupaten Mandailing Natal* (Doctoral dissertation, UNIMED).

[49] Satiawan, S. (2019). Investigasi Lapisan Akuifer Berdasarkan Data Vertical Electrical Sounding (VES) dan Data Electrical Logging; Studi Kasus Kampus Itera. *Bulletin of Scientific Contribution*, *17*(2), 91-100.

[50] Muhlisin, M. Z. (2019). *Identifikasi sebaran batubara menggunakan metode geolistrik polarisasi terinduksi (IP): Studi kasus daerah Klatak Kecamatan Besuki Kabupaten Tulungagung* (Doctoral dissertation, Universitas Islam Negeri Maulana Malik Ibrahim).

[51] Oyeyemi, K. D., Aizebeokhai, A. P., Metwaly, M., Omobulejo, O., Sanuade, O. A., & Okon, E. E. (2022). Assessing the suitable electrical resistivity arrays for characterization of basement aquifers using numerical modeling. *Heliyon*, *8*(5).

[52] Revil, A., Qi, Y., Barde-Cabusson, S., & Gresse, M. (2021). Induced polarization of the 1630-monogenetic dome, Furnas volcano, Sao Miguel Island, Azores archipelago. *Journal of Volcanology and Geothermal Research*, *420*, 107410.